Dissipative Dark Soliton in a Complex Plasma

R. Heidemann, S. Zhdanov, R. Sütterlin, H. M. Thomas, and G. E. Morfill
Max-Planck-Institut für extraterrestrische Physik, 85740 Garching, Germany
(Received 29 August 2008; published 31 March 2009)

The observation of a dark soliton in a three-dimensional complex plasma containing monodisperse microparticles is presented. We perform our experiments using neon gas in the bulk plasma of an rf discharge. A gas temperature gradient of 500K/m is applied to balance gravity and to levitate the particles in the bulk plasma. The wave is excited by a short voltage pulse on the electrodes of the radio frequency discharge chamber. It is found that the wave propagates with constant speed. The propagation time of the dark soliton is approximately 20 times longer than the damping time.

DOI: 10.1103/PhysRevLett.102.135002 PACS numbers: 52.27.Lw, 52.35.Mw, 52.35.Sb

We address the dynamics of nonlinear solitary waves which are impact excited in a dense complex plasma using a neon rf gas discharge at pressures 20–35 Pa. Complex plasmas are low pressure, low temperature plasmas containing microparticles. These microparticles are highly charged up by collecting plasma ions and electrons. They can be visualized individually with scattered light from a laser beam, which is recorded with a CCD camera.

The solitary wave structures we observe propagating in the complex plasma cloud are dominantly of a rarefactive type, hence resemble so called *dark solitons* (or *holes*, or *gray solitons* if mobile) important in a number of applications such as optical fibers, waveguides, laser beams, mechanics of discrete systems, etc. [1–4]. The physical mechanism determining the behavior of rarefactive solitary waves is still under debate [5]. Therefore, the search for physically realistic systems that can support stable solitary holes or dark solitons is of considerable interest [6]. Complex plasmas provide an excellent experimental system for such nonlinear structures.

There are two important points to be considered. First, nonlinear wave patterns observed in given experiments are highly dissipative. Therefore we will call them dissipative dark solitons (DDSs). Dissipativeness is ubiquitous, e.g., in granular media [7] which also can support solitary waves [8]. Second, DDSs are known to be weakly structurally unstable with a tendency to self-organize a shelf around the pulse wings [1]. In our case these are two asymmetric compressions that form the contour of the solitary wave. The backward one is a sedimentation front (similar to evaporation-condensation [9] or moisture wave fronts [10,11]). Here particle motion quickly damps and the cloud tends to restore its former quasiuniform structure. Note that the dissipative fronts are known as stabilizing factors for DDSs [6].

Travelling rarefactive structures are associated mostly with wave envelopes (as in examples with optic and waveguide applications cited above). Sound-like rarefactive waves are believed to be unstable. Nevertheless, a stable existence and propagation of compact rarefactive pulses is possible in multicomponent and nonisothermal plasmas, i.e., in conditions quite similar to those of our experiments. For example, rarefactive ion acoustic solitary waves have been observed in auroral plasmas [12], and in multicomponent plasmas with negative ions [13]. Soliton formation both of potential hill and potential dip type have been predicted to exist in multicomponent self-gravitating molecular clouds consisting of, for example, a hydrogen gas and a dust component or a mixture of normal matter and dark matter [14,15]. Especially for dust acoustic waves the opportunity to observe the rarefactive pulses has been discussed in [16,17]. Parameters of these waves were predicted to be strongly dependent on anisotropy, nonisothermality and gas pressure. Recently it has been shown that rarefactive longitudinal solitons in complex plasmas can be described by the extended Korteweg–de Vries equation [18,19]. Dissipative solitons, existing in open systems, are considered a natural extension of the soliton concept in conservative systems. Compared to classical solitons, they may evolve (i.e., change their shape [20]) during propagation.

Compressive solitons in 2D complex plasmas were observed and studied in [21]. These waves were excited by an electric pulse to a wire located approximately in the plane of the particle monolayer. Large amplitude dust acoustic waves and compressive shock like excitations in a 3D complex plasma were studied in [22–24]. Excitation was achieved using gas-dynamic impacts, or an electromagnetic impulse [24]. The complex plasma was confined by the strong electric field of dc discharge striations, and the observations used image intensity profiles.

We use a modified version [25] of the PK-3 Plus design [26] currently installed on board the International Space Station. Discharge pressures (20–35 Pa) were chosen in the under critical domain to avoid autowave excitations [25]—at a pressure below 20 Pa. This allowed us to achieve a stable single-wave regime (Fig. 1) involving no complications caused by the interaction of solitary and self-excited waves. Above 35 Pa the wave was too strongly damped to be observable. The rf effective voltage was set to 13 V, a very low value, just high enough to sustain the discharge.

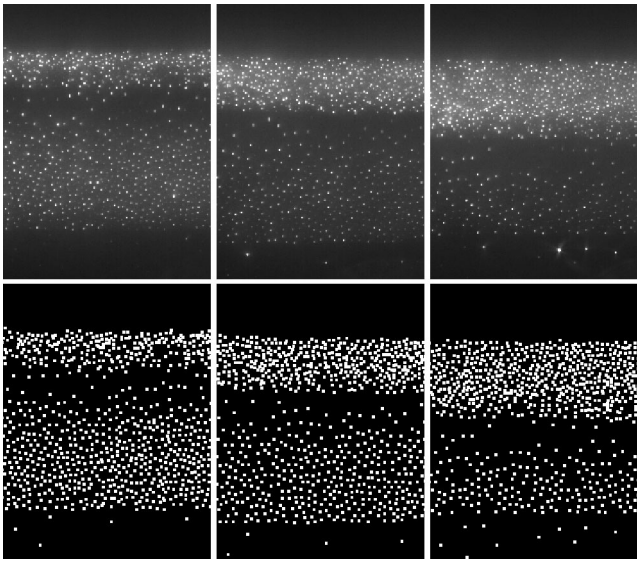

FIG. 1. Single-wave dynamics of the particle cloud. Upper row shows snapshots of the particle cloud. The cloud is illuminated by a laser beam extended to a sheet with the average thickness of 100 μm. The field of view is 13.7×7.2 mm^2. The brighter, growing stripe on the top of each image is the sedimented (nearly relaxed) part of the cloud. The bottom boundary of this stripe, expanding downwards, is the sedimentation front followed by the rarefaction zone (darker, almost particle free region below). From left to right: $t = 0.12$ s, 0.20 s, 0.28 s after the instant of shock excitation ($t = 0$ s). Neon gas pressure is 20.4 Pa. Tracked particle positions for the same time instants are shown in the lower row. Largely in-plane motion allows us to trace up to 95% of the particles in the field of view. Note that the rarefaction zone (*the dark soliton*) shifts rapidly downstream with respect to particle motion directed dominantly upwards [the maximal particle velocities (from left to right) are 1.8–2.0 cm/s].

Spherical monodisperse melamine-formaldehyde particles with a diameter of 3.42 ± 0.06 μm were injected into a neon plasma. To situate the particle cloud in the bulk plasma, slightly below the center, we used thermophoresis to almost balance gravity. The lower chamber flange was heated to establish a temperature difference of $\Delta T = 15$ K across the whole chamber. This elevates the particles above the plasma sheath. It also forestalls the formation of a void that would appear if gravity is balanced completely [27].

An approximately 100 μm thick vertical slice through the center of the complex plasma was illuminated by a diode laser. The scattered light was recorded under 90° by a high-speed camera with a frame rate of 1000 Hz. The resolution is 1024×1024 pixels. The used optics allowed us to observe an area of 27.4×27.4 mm^2 which resulted in a spatial resolution of 26.8 μm/px.

This camera and optics in combination with newly developed software allowed us to track the full motion of 95% of all particles during the experiment. This was impossible in earlier experiments [21–25]. To generate the dark soliton, the complex plasma was first compressed by a dc offset of 8.6 V externally applied to electrodes.

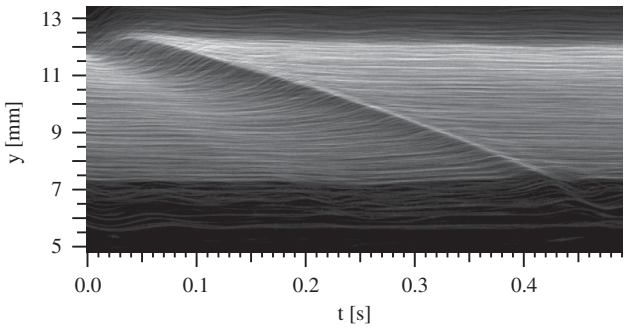

FIG. 2. Periodgram of the dark soliton in the complex plasma at 24.1 Pa. The wave is triggered by turning on or off a dc offset applied to both electrodes. The dark area corresponds to the rarefaction zone. The bright boundary on the right edge of the rarefaction zone is the narrow sedimentation front behind the wave. The periodgram is constructed from 490 still images (0.49 s). The vertical axis shows the distance from the lower electrode. The center of the plasma chamber is at 15 mm.

Switching off the dc offset triggers a solitary rarefaction wave. Particles are accelerated inside the wave, then decelerate forming a sedimentation front where the particles relax into a new equilibrium configuration (Fig. 1).

Figure 2 illustrates the propagation of the dark soliton through the particle system. In our recorded images the dark soliton propagates vertically (y direction), and the particle distribution in horizontal x direction is almost homogeneous (Fig. 1). The local particle density is proportional to the local visible brightness in the images. For each image the brightness is averaged in x direction resulting in a line showing the vertical brightness distribution. The periodgram is constructed by stacking these lines together, representing the temporal evolution of the vertical brightness distribution in the recorded images, and thus the density of the particle cloud. The dynamical scenario of the wave pattern formation is as follows: first, immediately after switching off the negative voltage offset, the particles are at rest; next, the top layer accelerates into the empty region above the particle cloud, quickly followed by the second and further layers. These fast moving particles constitute the rarefaction zone. They are stopped suddenly, forming a sedimentation front. At low pressures (<24 Pa) the fast particles can penetrate trough the sedimentation front for up to five particle layers, resulting in a bidirectional flow. From tracked particle trajectories we calculate the particle number distribution $N_y(t)$ using a sliding window technique. The particles are counted in a window 1024×8.5 pixel^2 centered around a given point y. This window is shifted in y direction in 2 pixel steps. As a reference for these particle number distributions we determined the distribution of particle numbers in the undisturbed cloud $\langle N_y \rangle_t$ at the same discharge conditions. The reference distribution is obtained by averaging over a time interval of 1 s (i.e., over 1000 frames). $N_y(t)$ and $\langle N_y \rangle_t$ are shown in Fig. 3(a).

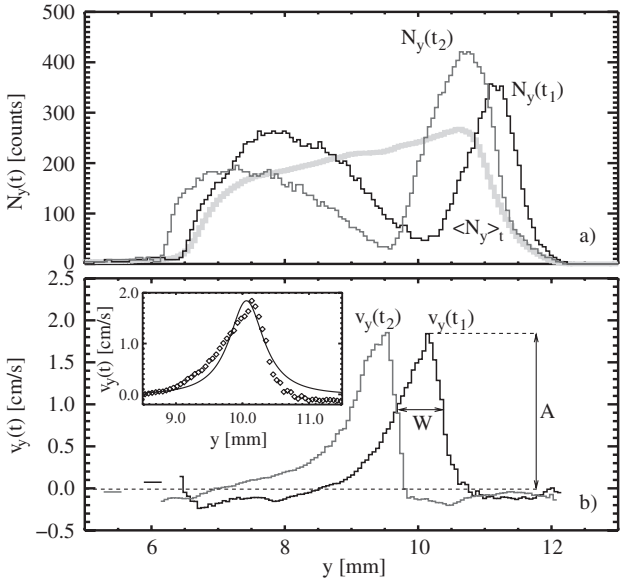

FIG. 3. (a) Particle number distributions $N_y(t)$ and (b) vertical particle velocity profiles $v_y(t)$ vs vertical position y, measured at 20.4 Pa and at $t_1 = 0.12$ s, $t_2 = 0.20$ s after the instant of excitation. The distribution of the undisturbed cloud $\langle N_y \rangle_t$ is drawn in grey. The mean interparticle separation is $\Delta \approx 90$ μm. The arrows indicate the amplitude (A) and the width at a half amplitude (W). Note that the minima of $N_y(t)$ correspond to the maxima of $v_y(t)$. (insert) The DDS velocity profile [5,34] matches well to the observed one (the fit accuracy is $\sigma =$ 1.9 mm/s). The fit parameters were taken from the experiment at $t = t_1$.

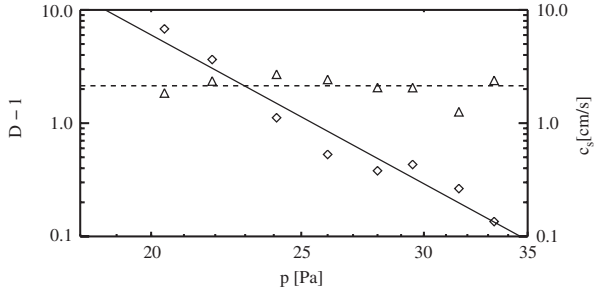

FIG. 4. (diamonds) Average maximum decompression ratio D and (triangles) the speed of sound c_s vs neon gas pressure. The solid line shows the power law least square fit: $D = \alpha(p[\text{Pa}]/20)^n + 1$, $\alpha = 6 \pm 1$, $n = -7.5 \pm 0.7$. The speed of sound was obtained by using the well-known relationship [5,34] $c_s = A\frac{\sqrt{D}}{D-1}$. The speed of sound depends weakly on pressure as the theory [17] predicts. On average, there is $\langle c_s \rangle = 2.14 \pm 0.16$ cm/s (the dashed line).

The particle number distributions have three distinct large scale features: two maxima and one minimum. Close to the maxima the cloud is evidently denser compared to the reference distribution $\langle N_y \rangle_t$. These maxima are easy to identify: The first one (at lower y values) is the initial compression, which forms before the wave starts to propagate. The second one (at higher y values) corresponds to the sedimented part of the cloud, slowly relaxing into the new quasiequilibrium position. We identify the rarefaction zone between the maxima as the dark soliton. The rear edge of the dark soliton is steeper than the front edge.

To characterize the strength of the wave using these particle distribution functions, we determine the average maximum decompression ratio D. First we calculate the ratio $d(y, t) = \frac{\langle N_y \rangle_t}{N_y(t)}$, from which we select the maximum for each frame, and then average the result over the whole image sequence. With increasing pressure the decompression ratio decreases (Fig. 4). So the wave gets weaker with higher pressure, which is expected because of the higher neutral gas drag.

Averaged vertical particle velocity profiles $v_y(t)$ are shown in Fig. 3(b). Note that inside the wave the particles accelerate upwards, that is in the opposite direction compared to the soliton propagation direction. Using these profiles we define three parameters of the wave (see Fig. 5): amplitude, speed, and width.

The shape of the dark soliton depends on the neutral gas pressure. The highest observed initial amplitude is $A_{\text{init}}(20.4\ \text{Pa}) = 4.50 \pm 0.03$ cm/s. In the range of 20–30 Pa the initial width of the wave is independent of pressure and has an average value of $\langle W_{\text{init}} \rangle = 0.69 \pm 0.05$ mm. The shape of the wave changes while it propagates through the cloud. For different neutral gas pressures the deformation dynamics varies. During the short

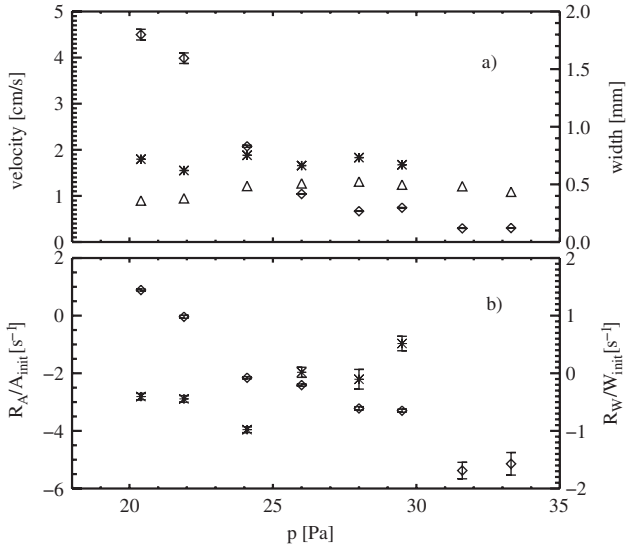

FIG. 5. (a) The dark soliton's amplitude A_{init} (diamonds), the width W_{init} (stars), and the wave speed v_{DS} vs pressure determined shortly after the instant of excitation. At pressures above 30 Pa the wave is too weak to determine its width properly. (b) The initial rate of the relative amplitude variation R_A/A_{init} (diamonds) and the relative width variation R_W/W_{init} (stars). Note that at $p < 22$ Pa the amplitude rate is positive, indicating a weak instability of the wave.

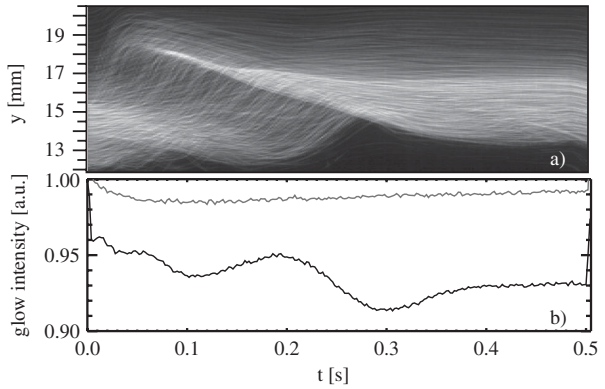

FIG. 6. (a) The particle number density profile and [(b), the black curve] the complex plasma glow intensity vs time. Apparently, the variation in the plasma glow follows the particle density variation. [(b), the gray curve] A control measurement in the particle-free plasma shows no such activity. The wave is triggered by turning on or off a dc offset applied to the bottom electrode.

time ($\sim$0.3 s) that we observe the propagating waves their amplitude and width vary approximately at a constant rate $R_A = \frac{dA}{dt} = \text{const}$, $R_W = \frac{dW}{dt} = \text{const}$, these constants are dependent on pressure. The relative variations R_A/A_{init} and R_W/W_{init} normalized by the initial values of the amplitude and the width, determined shortly after the instant of wave excitation, are shown in Fig. 5(b).

Surprisingly for $p < 22$ Pa the amplitude rate is positive, and the amplitude of the wave increases with time. The relative width variation is negative in this interval. Hence, the soliton's shape gets steeper. Since the complex plasma cloud is globally stable, this weak instability could be due to the nonlinear global modes [25,28]. Note also a well pronounced correlation of variations in the cloud density associated with DDS and in the plasma glow (Fig. 6). Note also that the enhanced discharge glow in the regions of the reduced particle number density favors the ionization instability [29,30].

At pressures above 22 Pa the soliton amplitude decreases rapidly during the propagation time, exactly as one would expect for waves propagating in any dissipative medium. However, the soliton amplitude decay rate is at least 10–25 times lower than the Epstein damping rate [31]. Such an anomalously low wave damping rate has also been found in plasma crystals previously [32,33]. It is thought to be due to a collective effect but an explanation is still outstanding.

To conclude, a rarefactive strongly nonlinear solitary wave has been excited in a dense complex plasma cloud compensated for gravity by thermophoresis. The rarefaction zone was observed traveling at a speed $\sim$2 cm/s. We identify this wave as *a dissipative dark soliton* (with decompression factor as large as 7.8). We observed that the DDS could self-support its propagation for as long as tens of dissipation times at least. The excitation and free propagation of this nonlinear dissipative structure can be observed because the complex plasma is in an active undercritical state for the pressure range used in the experiments.

This research was funded by DLR/BMWi Grant No. 50WP0203. Special thanks to Dr. Konopka and Peter Huber for continuous support in data analysis and programming, and Dr. Rothermel and Dr. Konopka for valuable help with planning and building the experiment.

[1] S. Burtsev *et al.*, J. Opt. Soc. Am. B **14**, 1782 (1997).
[2] Y. S. Kivshar, Phys. Rev. A **43**, 1677 (1991).
[3] B. C. Collings *et al.*, Opt. Lett. **22**, 1098 (1997).
[4] N. K. Efremidis *et al.*, Phys. Rev. E **66**, 046602 (2002).
[5] A. Hasegawa *et al.*, *Optical Solitons in Fibers* (Springer-Verlag, Berlin, 2002).
[6] N. Efremidis *et al.*, Phys. Rev. E **62**, 7410 (2000).
[7] P. B. Umbanhowar *et al.*, Nature (London) **382**, 793 (1996).
[8] A. Snezhko *et al.*, Phys. Rev. Lett. **94**, 108002 (2005).
[9] O. Inomoto *et al.*, Phys. Rev. Lett. **85**, 310 (2000).
[10] V. S. Shklyar *et al.*, J. Eng. Phys. Thermophys. **11**, 261 (1966).
[11] J. Carmeliet *et al.*, J. Therm. Envelope Build. Sci. **27**, 277 (2004).
[12] S. S. Ghosh *et al.*, Nonlinear Proc. Geophys **11**, 219 (2004).
[13] Y. Nakamura *et al.*, Phys. Rev. Lett. **52**, 2356 (1984).
[14] T. Cattaert *et al.*, Astron. Astrophys. **438**, 23 (2005).
[15] R. E. Kates *et al.*, Astron. Astrophys. **206**, 9 (1988).
[16] A. A. Mamun, Phys. Rev. E **55**, 1852 (1997).
[17] P. K. Shukla *et al.*, *Introduction to Dusty Plasma Physics* (IOP, Bristol, 2002).
[18] I. Kourakis, in *Multifacets of Dusty Plasmas: ICPDP5*, AIP Conf. Proc. No. 1041 (AIP, New York, 2008).
[19] I. Kourakis *et al.*, Eur. Phys. J. D **29**, 247 (2004).
[20] N. Akhmediev *et al.*, *Dissipative Solitons. Lect. Notes Phys.* (Springer, New York, 2005), Vol. 661.
[21] D. Samsonov *et al.*, Phys. Rev. Lett. **88**, 095004 (2002).
[22] V. E. Fortov *et al.*, Phys. Plasmas **10**, 1199 (2003).
[23] V. E. Fortov *et al.*, Phys. Rev. E **69**, 016402 (2004).
[24] V. E. Fortov *et al.*, Phys. Rev. E **71**, 036413 (2005).
[25] M. Schwabe *et al.*, Phys. Rev. Lett. **99**, 095002 (2007).
[26] H. M. Thomas *et al.*, New J. Phys. **10**, 033036 (2008).
[27] H. Rothermel *et al.*, Phys. Rev. Lett. **89**, 175001 (2002).
[28] A. Couairon *et al.*, Physica (Amsterdam) **108D**, 236 (1997).
[29] N. D'Angelo, Phys. Plasmas **5**, 3155 (1998).
[30] X. Wang *et al.*, Phys. Plasmas **8**, 5018 (2001).
[31] P. S. Epstein, Phys. Rev. **23**, 710 (1924).
[32] M. Rubin-Zuzic *et al.*, New J. Phys. **9**, 39 (2007).
[33] M. Rubin-Zuzic *et al.*, Nature Phys. **2**, 181 (2006).
[34] P. O. Fedichev *et al.*, Phys. Rev. A **60**, 3220 (1999).